Readout Models for General Electric BAS-MS Image Plates

Introduction

The performance of inertial confinement implosions on OMEGA is potentially limited by the production of hot electrons.[1] The hard x-ray image-plate (HXIP) diagnostic[2] is used to determine the energy distribution of the hot electrons by estimating the spectrum of the x rays that are generated through bremsstrahlung with the target. Simulations and data from this diagnostic agree with a bi-Maxwellian shape for the total time-integrated hot-electron spectrum, which for low-Z targets generates an x-ray energy spectrum that is approximately the sum of two exponentials.[3]

HXIP is a time-integrated multichannel x-ray spectrometer. X rays incident on the detector are attenuated by different high-pass filters for each channel and are then recorded by a General Electric (GE) BAS-MS image plate,[4] whose active layer is $BaFBr_{0.85}I_{0.15}:Eu^{2+}$ and is structured as described in Table 152.I. After an experiment, the image plates are removed from the detector and the photostimulated luminescence (PSL) is scanned out by a Typhoon FLA 7000 flying spot scanner. Since the initial signal level for some channels is often higher than the saturation limit of the scanner, image plates are repeatedly scanned until all signal levels are below saturation.

The signal on image plates fades both with time and through readout. The time fading of BAS-MS image plates has been characterized by Ohuchi and Hatano, who measured the signal fading given elapsed time and ambient temperature.[6] The decay rate of the signal on an image plate based on readout number alone has been estimated several times, although never for the BAS-MS image plate with the Typhoon FLA 7000 scanner.[7–9] A model covering the relationship between the depth of deposited energy and the contribution to signal was provided by Bonnet *et al*., who exponentially weighted the deposited energy distribution with a falloff length.[10] Thoms provides a theoretical model of the readout process over any number of scans based on the photon diffusion equation and finds a triple exponential decay for PSL centers as a function of integrated photon flux.[11–13]

Image-plate scan sequences for HXIP indicate a small variation in fade ratio (defined as the current signal value divided by the preceding signal value) between channels and a larger variation between different experiments. A data set of 200 scan sequences for HXIP with at least two scans (see, for example, Fig. 152.11) is used to determine the parameters for a new model of the readout fading.

The following sections: (1) explain the nonapplicability of existing image-plate models to the BAS-MS image plate; (2) derive two basic image-plate models; (3) present methods of determining the model parameters from the HXIP experimental data; and (4) discuss the results.

Table 152.I: Layers of a BAS-MS–type image plate. The first four columns are transcribed from vendor documents.[5] The empirical formulas are calculated from the fifth column, using estimates for unknown values such as the composition of "plastic."

Layer	Width (μm)	Material	Density (g/cm^3)	Calculated empirical formula
Surface	9	Polyethylene terephthalate (PET)	1.4	$C_{10}H_8O_4$
Phosphor	115	25:1 mix $BaFBr_{0.85}I_{0.15}$:urethane	3.3	$Ba_{2263}F_{2263}Br_{1923}I_{339}C_{741}H_{1730}N_{247}O_{494}$
Back	12	Plastic	1.4	$C_{10}H_8O_4$
Base	190	PET	1.4	$C_{10}H_8O_4$
Ferrite	80	MnO, ZnO, Fe_2O_3, plastic	3.0	$Mn_{1015}Zn_{885}Fe_{902}C_{1315}H_{1315}O_{4568}$
Back protective	25	PET	1.4	$C_{10}H_8O_4$

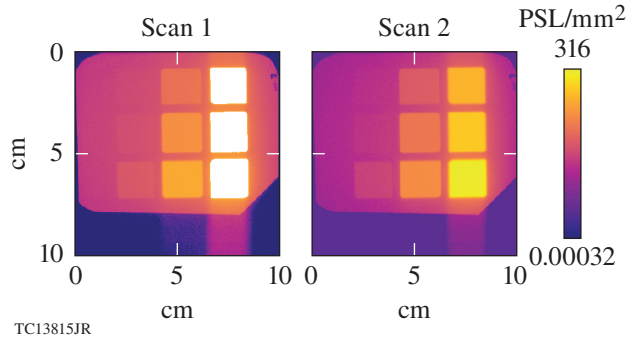

Figure 152.11
Two successive image plate scans for the wide-aperture hard x-ray image plate (HXIP) configuration. Some channels are initially saturated.

Image-Plate Models

1. Review of Existing Image-Plate Models

A first model for the readout process for image plates was derived by Thoms[11] and later extended to include a triple-exponential fading function for the excitation centers in the image plate, which are referred to as photostimulable F-centers.[12] Photon propagation in the image plate is modeled using a 3-D photon diffusion equation and solved numerically. While this may be appropriate for the Fuji ST III image plate for which parameters were determined,[12] the light transport equation used requires that (1) photons are scattered isotropically, (2) the absorption length is much larger than the scattering length, and (3) the scattering length is small compared to the sensitive layer thickness so that photons can immediately be treated as diffuse. Since the estimated parameters for a $BaFBr_{0.85}I_{0.15}$:Eu image plate that are similar in structure to the BAS-MS indicate significant absorption and weak and anisotropic scattering of photons,[14] this model is not applicable.

A variation on the Thoms model using the four-flux model[15] for light transport comes from Masalovich *et al.*, who considered KCl:Eu and KBr:Eu image plates.[16] The four-flux model invokes fewer assumptions than the photon diffusion equation used by Thoms,[11] although it requires the F-center distribution to be uniform along all but the depth coordinate. The four-flux model is used to estimate the readout light flux distribution and the PSL escape probability, from which the image-plate response can be calculated. Since readout light and PSL have different wavelengths, the many free parameters for the four-flux model must be specified for both wavelengths. In practice, the two functions can usually be approximated by much simpler linear or exponential functions.

Finally, Vedantham and Karellas[14] construct a comprehensive image-plate model with more than 20 parameters that relies on simulations of photon transport, taking into account grain sizes and binder material within the image plate. If all the parameters were measured and the structural assumptions of the optical simulations were correct, the model would be appropriate for the BAS-MS image plate. However, many of the model parameters were measured for BaFBr:Eu and assumed to match for $BaFBr_{0.85}I_{0.15}$:Eu, and most information on the internals of the BAS-MS image plate has been kept proprietary.

2. Image-Plate Readout Process

Two image-plate models are introduced in the following sections. In the fixed-distribution model, it is assumed that the shape of the distribution of F-centers in the image plate at any time is unchanged and only its magnitude decreases. In the fading-distribution model, the fading of the F-center distribution as a function of time and depth is structured around the interaction of laser photons and F-centers, which generates PSL.

Figure 152.12 summarizes the readout process of a given distribution $\eta(z)$:[1/mm^3] of F-centers within the image plate's sensitive (phosphor) layer. Laser photons at 650 nm pass into the sensitive layer from the front of the image plate, and the photon flux $\phi(z)$ is reduced (by absorption or scattering) deeper in the image plate. A single cross section σ:[cm^2] describes the interaction between laser photons and the photostimulable F-centers to produce a 390-nm photon and remove an F-center.

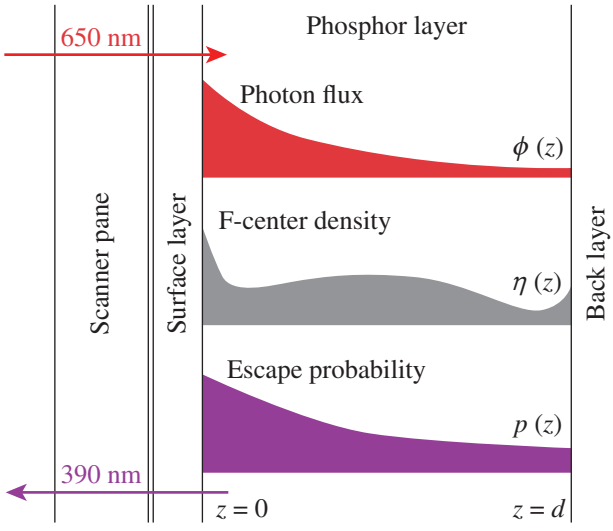

Figure 152.12
Typical shapes of the photon flux distribution, F-center density distribution, and photostimulated luminescence (PSL) escape-probability function within the sensitive layer of an image plate.

[Note that $F(Br^-)$ and $F(I^-)$ centers are treated identically.] The density $\eta(z)$ is assumed to be small enough that absorption by F-centers does not significantly alter the laser photon flux. PSL generated at a given depth z escapes the image plate and is recorded by the scanner optics with probability $p(z)$.

Because a detailed and accurate optical analysis of the BAS-MS plates is difficult, the readout laser photon flux can instead be approximated by the function

$$\phi(z) = Ie^{-z/L_R}, \tag{1}$$

which is defined over $z \in [0,d]$ for the d sensitive layer depth. I:[1/cm^2 • s] is the average photon flux density at the surface of the sensitive layer and L_R is a length factor accounting for the readout photon scattering and absorption effects within the sensitive layer. Similarly, the escape probability can be approximated by

$$p(z) = \frac{1}{2}e^{-z/L_B} \tag{2}$$

in which L_B is another length factor accounting for PSL photon scattering and absorption in the sensitive layer. The F-center distribution $\eta(z)$ can be estimated by assuming that the density of F-centers is proportional to the energy deposited by incident high-energy particles. Separate proportionality constants may apply for each particle type.[10]

3. Fixed-Distribution Model

Under the fixed-distribution model, the total signal S_1 for the first scan is

$$S_1 \propto \int_0^d \phi(z)\sigma\eta(z)p(z)\mathrm{d}z, \tag{3}$$

where σ:[cm^2] is the cross section of photostimulated luminescence with an F-center. Because both $p(z)$ and $\phi(z)$ contain exponentials, defining a combined absorption and scattering length $L = \left(L_R^{-1} + L_B^{-1}\right)^{-1}$ reduces this expression to

$$S_1 = \alpha\int_0^d \eta(z)e^{-z/L}\mathrm{d}z. \tag{4}$$

The factor α:[PSL] is a scale factor encompassing the cross section σ, average laser photon flux density I, illumination time τ, the factor 1/2 from $p(z)$, and the conversion from photostimulated luminescence photons to FLA 7000 intensity units (which are also labeled "PSL").

To account for readout fading, the fixed-distribution model uses an empirical fading formula that has been used for other scanner and image-plate combinations.[7–9] The signal for the nth scan is then

$$S_n = S_1\prod_{i=2}^{n}\left[f_{max} - \left(f_{max} - f_{min}\right)e^{-(i-2)/\mathcal{T}_{fade}}\right]. \tag{5}$$

The fade ratio S_n/S_{n-1} decays exponentially with time. For the first two scans, the fade ratio is f_{min}; for large n it approaches f_{max}; and in between, the falloff in fade ratio has an exponential time constant $\mathcal{T}_{fade}$.

The controlling parameters for the fixed-distribution model are the minimum and maximum fade ratios f_{min} and f_{max}, time constant $\mathcal{T}_{fade}$, falloff length L, and scale factor α.

4. Fading-Distribution Model

In the fading-distribution model, the F-center distribution $\eta(z)$ changes with readout time according to

$$\frac{d}{dt}\eta(z) = -\phi(z)\sigma\eta(z). \tag{6}$$

If τ is the total readout time for a given area over a single scan, the change in the number of F-centers during the nth scan is

$$\eta(z)\left[e^{-(n-1)\sigma\tau\phi(z)} - e^{-n\sigma\tau\phi(z)}\right], \tag{7}$$

where $\phi(z)$ is the photon flux-density approximation from Eq. (1). Since the change in the F-centers equals the PSL generation, the nth scan signal is

$$S_n = \beta\int_0^d \eta(z)w_1(z)e^{(n-1)\sigma\tau\phi(z)}\mathrm{d}z, \tag{8}$$

$$w_1(z) = p(z)\left[1 - e^{-\sigma\tau\phi(z)}\right], \tag{9}$$

where β:[PSL] is a scale factor including the PSL photon to scanner PSL conversion and a factor 1/2 from $p(z)$, which in Eq. (2) gives the PSL escape probability.

The fading-distribution model expression for the first scan signal reduces to Eq. (4) when the number of readout photons is small [$\phi(z)\sigma\tau \ll 1$]. The empirical time decay formula in Eq. (5) can be derived as an approximation for small n if the shape of $\eta(z)$ is fixed, although the expression for $\mathcal{T}_{fade}$ is complicated.

The fading-distribution model is parameterized by falloff lengths L_R and L_B, scale factor β, and unitless product $I\sigma\tau$

encompassing the average incident photon flux density I [see Eq. (1)], F-center cross section σ, and illumination time τ.

Parameter Estimation

1. Scanner-Induced Image-Plate Errors

The Typhoon FLA 7000 scanner used to scan the image plates uses GE software, 50-μm resolution, a 650-nm laser, and a special calibration procedure as described in Williams *et al.*[17] As a result of a lossy conversion from exponential scaling to the offset quadratic scale used by the scanner software, precision at low intensities is reduced. Time fading is not an issue, however, for the HXIP data set: over the 90 s used to scan a 10-cm × 10-cm region, the change in signal caused by time fading is less than 1% for scans begun at least 20 min after exposure.

Streaking effects along one axis of the HXIP images are visible below the image plate boundaries in Fig. 152.11. One possible explanation is that stray readout laser light (possibly reflecting off the front image-plate surface or off scanner components) interacts with regions of the image plate far away from the currently illuminated spot. Only the generated PSL aligned with the light guide of the scanner is recorded, so that the signal at a given location is proportional to the F-center density at that location plus a small fraction of the F-center density along the scan line. If this hypothesis is correct, the streaking effects are linear and can be accounted for.

2. Bounds on Parameter Values

Bounds on the model parameters can be determined using extremal values from the HXIP data set. In this example and for all other parameter estimation, the signal values have been corrected for time fading (assuming a constant 20°C temperature).[6] The observed maximum fade ratio between successive scans is 0.85 for the change in channel signal from the 11th to the 12th scan of a scan sequence, and the minimum fade ratio is 0.15, measured for the least-filtered channel between the first and second scans.

If the time-fading correction does not introduce any significant errors, then for the image-plate readout models to be consistent with this information, the entire range of fade ratios from 0.15 to 0.85 must be attainable for some F-center distribution. For the fixed-distribution model, this condition requires that the parameters $f_{\min} < 0.15$ and $f_{\max} > 0.85$. With the fading-distribution model, the minimum-possible fade ratio $\mathcal{F}_{\min} < 0.15$ is obtained for an F-center distribution concentrated at the front of the sensitive layer [$\eta(z) = \delta(z)$] and the maximum $\mathcal{F}_{\max} > 0.85$ for a concentration at the back of the layer [$\eta(z) = \delta(z–d)$]. Evaluating the fading-distribution model for these two extreme cases yields $I\sigma\tau = -\log \mathcal{F}_{\min} > 1.9$ and $L_{\mathrm{R}} = d \Big/ \log\left(\log \mathcal{F}_{\max} \Big/ \log \mathcal{F}_{\min}\right) < 100\ \mu$m. The parameter L_{B} cannot be determined without constraining the shape of the depth distribution of the F-centers.

3. Determining Parameters by an Error Minimization Fit

For a given model m, the model parameters Ω_m are determined by minimizing the errors between the available data and a fit to that data based on the assumption that the x-ray energy spectra incident on HXIP are sums of two exponentials. The average error χ_s^2 for a specific scan sequence s is computed using

$$\chi_s^2 = \sum_{\substack{n \in \text{scans} \\ c \in \text{scans}}} w_{\mathrm{c}} \left(\log \frac{v_{n,c}\left[\Psi_s;\Omega_m\right]}{x_{s,n,c}} \right)^2, \tag{10}$$

where w_c is a weight inversely proportional to the number of scans for which a channel is neither saturated nor read out below the noise threshold. The values $x_{s,n,c}$ are the measured signals for scan sequence s, the nth scan, and the cth channel. The function $v_{n,c}[\Psi_s;\Omega_m]$ calculates the expected channel signal as a function of scan sequence parameters Ψ_s and model parameters Ω_m [see the **Appendix** (p. 190) for details]. The mean square log deviation is chosen as a measure of error because the data are always positive and often a factor of 2 distant from the fit values, so the assumption of normally distributed errors under which minimizing squared (linear) errors yields a maximum-likelihood solution does not apply.

Because the errors χ_s^2 have a long-tailed distribution, the geometric mean is used to combine them into a single cost function C, over which the model parameters Ω_m can be minimized. (The arithmetic mean would overemphasize scan sequences whose errors are large for reasons unrelated to the readout model; using it shifts the final model parameter estimates only slightly). Therefore,

$$C = \sqrt[N_s]{\prod_{s \in \text{seqs}} \left(\chi_s^2\right)}, \tag{11}$$

where N_s is the number of scan sequences used for the fit.

Due to the large number of total parameters, the fit procedure is performed in two loops: in the outer loop, the minimi-

zation over model parameters Ω_m uses a global optimization method for C based on a surrogate function using linear interpolation on a Delaunay triangulation;[18] in the inner loop, for each scan sequence, the values Ψ_s minimizing χ_s^2 are found by brute force followed by gradient descent. The simplex mesh surrogate is chosen because it can handle both fine detail (near the minima) and coarse detail (for the global shape) without requiring tuning. Computations on the surrogate are efficient since they reduce to computations on linear functions.

Applying the fit procedure to the fixed-distribution and fading-distribution models over a data set of 212 image-plate scan series with at least two scans provides the model parameters and error measures given in Table 152.II. The error bars and limits on individual parameters are computed from the region of parameter space where the surrogate function is less than $1.1C$. An alternative approach to estimating the error for the parameters is to minimize C repeatedly, each time using a variation on the original data set perturbed according to the measurement errors of each value, and use the distribution of parameters found to compute the error for each parameter. For the HXIP data set, such Monte Carlo error estimation yields extremely narrow error bars when only accounting for statistical errors. Accurately modeling the systematic errors involved in the estimation of $v_{n,c}[\Psi_s;\Omega_m]$ is beyond the scope of this article.

Table 152.II: Best-fit parameters for the fixed-and fading-distribution models. See **Determining Parameters by an Error Minimization Fit** (p. 187) for an explanation of the error bars and bounds.

Model	Parameters	Bounds
Fixed distribution	$f_{\max} = 0.83 \pm 0.10$	(0.65,1.00)
	$f_{\min} = 0.36 \pm 0.02$	(0.35,0.38)
	$\mathcal{T}_{\text{fade}} = 3.75 \pm 1.0$	(0.31,11.0)
	$L = 136 \pm 43\ \mu$m	(39 μm, ∞)
Fading distribution	$I\sigma\tau = 2.8 \pm 0.3$	(2.3,3.3)
	$L_{\text{B}} = 220 \pm 90\ \mu$m	(200 μm, 680 μm)
	$L_{\text{R}} = 51 \pm 28\ \mu$m	(39 μm, 136 μm)

Plotting the minimum C while fixing a single parameter at a time does not capture the complex trade-off between parameters; see Fig. 152.13 for the minimum model errors when fixing two of the parameters. The practical difference between best-fit models is shown in Fig. 152.14. The scale factors α and β for the two models cannot be determined since the absolute intensity of the x rays recorded by HXIP is uncertain.

Discussion

The fading-distribution model yields a significantly lower average error ($C = 0.133$) than the fixed-distribution model ($C = 0.170$). Since the cost function C is a relative measure, neither value implies a quantifiable certainty in the parameter values. However, C can be used as a proxy for the likelihood of a given combination of model parameters, assuming the model in question is correct.

For instance, with the fading-distribution model, L_{R} is constrained to the range (39 μm, 136 μm). While lower values of L_{R} do not significantly increase C, they are unphysical, especially for L_{R} less than the phosphor particle size of 5 μm (Ref. 4). For large L_{R}, the error increases up to the point where the fading-distribution model reduces to a simpler one with a fixed fade ratio. The other length parameter L_{B} induces only gradual changes in error as it varies; it follows that the minimization of C only weakly constrains L_{B}. To determine L_{B} with any more precision would require a different method of estimation. The combined parameter $I\sigma\tau$, which encompasses the photon flux, PSL cross section, and illumination time, has estimated bounds $2.3 \lesssim I\sigma\tau \lesssim 3.3$, outside which L_{R} and L_{B} can no longer effectively compensate for the extreme value of $I\sigma\tau$.

The interaction between parameters for the fixed-distribution model is more complicated, but it is also more clearly influenced by features of the HXIP data set. For instance, most of the scan sequences available are between two and five scans in length. The variation in fade ratios between channels and between scan sequences is largest for the initial scans and smaller for the final scans in a sequence. As Fig. 152.13 shows, C quickly increases on deviating from the minimized $f_{\min} = 0.36 \pm 0.02$. The error on $f_{\min}$ is small since changes to it directly alter the first fade ratio for about 200 scan sequences. Meanwhile, fade ratios approaching $f_{\max}$ are obtained only for the few sequences with more than five scans, and correspondingly the change in C is more gradual, yielding a larger error on $f_{\max} = 0.83 \pm 0.10$. The bias toward short scan sequences also affects parameter $\mathcal{T}_{\text{fade}}$ since for the first three or four scans in a sequence, increasing $\mathcal{T}_{\text{fade}}$ in conjunction with $f_{\max}$ only slightly increases C. Finally, without the influence of differing fade ratios on the length parameter (as for the fading-distribution model), the value of C is largely independent of L, whose value, like that of L_{B}, must be determined by another method.

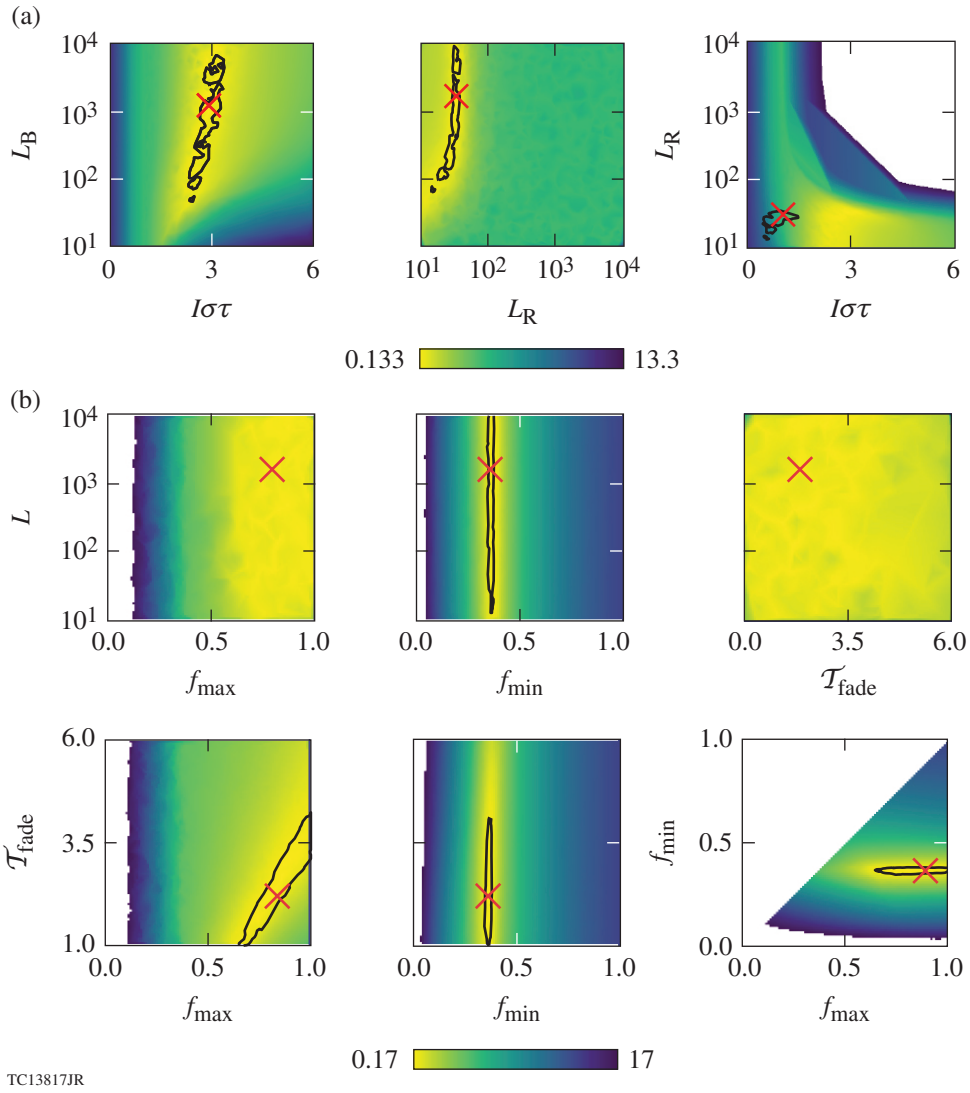

Figure 152.13
Plot of the cost function C for the (a) fading-distribution model and (b) fixed-distribution model when two parameters are fixed and the rest are minimized. The black line is the contour of the surrogate function at $1.1C$, and × marks the minimum. The contour is omitted where it is too convoluted.

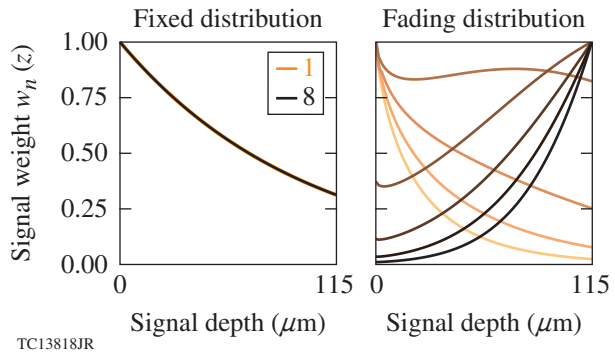

Figure 152.14
Normalized weight functions $w_n(z)$ for the two models defined so that the equation $S_n = \alpha_n \int_0^d w_n(z)\eta(z)\mathrm{d}z$ describes the nth scan signal S_n as a function of the F-center distribution $\eta(z)$ in the image plate, where α_n is a scale parameter. For the fixed-distribution model, all normalized weight functions are identical.

Not all inferred model parameters agree with previous work on the BAS-MS image plate. For instance, the fading-distribution model parameter $L_R = 51 \pm 28\ \mu m \in (39\ \mu m, 136\ \mu m)$ implies strong attenuation of the incident readout laser. Although the fading-distribution and fixed-distribution models have different equations, the distorting effect of the depth-dependent fading is small enough for the first scan only that the parameters of the two models can be compared to find $L \approx \left(L_R^{-1} + L_B^{-1}\right)^{-1}$, which implies $L \lesssim L_R$. Both the length $L = 125 \pm 35\ \mu m$ from Boutoux *et al.*[19] and the length $L = 222 \pm 72\ \mu m$ found by Bonnet *et al.*[10] are higher than expected given the value of L_R. Moreover, the error plot in Fig. 152.13 indicates that while smaller L_R values are plausible, larger values of L_R significantly increase the average error.

Conclusion

In summary, a simple model for BAS-MS image plates that accounts for readout fading has been proposed and found to improve the Bonnet *et al.* model[10] combined with an empirical treatment of readout fading. Model parameters are inferred that minimize errors on a collection of experimental HXIP data. The model implies that the response of the second image-plate scan may not be proportional to the response of the first scan, especially when large variations in the depth distribution of F-centers within the image plate are present. The procedure to determine model parameters accurately determines fading parameters but yields little certainty on values related to the transportation of PSL photons and cannot provide any of the scale factors involved in an absolute calibration.

ACKNOWLEDGMENT

The authors thank D. Edgell and C. Stoeckl for insightful discussions.

This material is based upon work supported by the Department of Energy National Nuclear Security Administration under Award Number DE-NA0001944, the University of Rochester, and the New York State Energy Research and Development Authority.

Appendix: Estimating Signal Values for a Specific Scan Sequence

The expected signal for channel c of scan n of sequence s given model parameters Ω_m and spectrum parameters Ψ_s, $v_{n,c}[\Psi_s;\Omega_m]$ are defined as a product of operators,

$$v_{n,c}\left[\Psi_s;\Omega_m\right] = \mathcal{I} \times M_n\left[\Omega_m\right] \times R_{c,s} \times \left[f\left(E;\Psi_s\right)\right], \quad \text{(A1)}$$

where $\mathcal{I}$ approximates the additional signal from F-centers in different regions of the image plate caused by stray readout light in the scanner. This correction is performed on estimated signals rather than the image plates themselves in order to avoid negative values. $M_n[\Omega_m]$ provides the signal recorded by the scanner for a given depth distribution of F-centers, using the formulas derived in **Image-Plate Models** (p. 185). $R_{c,s}$ converts an arbitrary x-ray spectrum to the resulting depth distribution $\eta(z)$ within the region of the image plate corresponding to the channel. It is calculated for each HXIP configuration using a *Geant*[20] simulation of the detector. The simulation accounts for backscattering from the aluminum image-plate holder and Compton-scattered photons from the channel filters, which contribute to the F-center distribution in other channels' regions of interest. Finally, $f(E;\Psi_s)$ is the approximated x-ray energy spectrum given by

$$f\left(E;\Psi_s\right) = A_1 e^{-E/kT_1} A_2 e^{-E/kT_2}, \quad \text{(A2)}$$

where A_1, A_2, kT_1, and kT_2 are the spectrum parameters encompassed by Ψ_s.

REFERENCES

1. D. H. Froula, D. T. Michel, I. V. Igumenshchev, S. X. Hu, B. Yaakobi, J. F. Myatt, D. H. Edgell, R. Follett, V. Yu. Glebov, V. N. Goncharov, T. J. Kessler, A. V. Maximov, P. B. Radha, T. C. Sangster, W. Seka, R. W. Short, A. A. Solodov, C. Sorce, and C. Stoeckl, Plasma Phys. Control. Fusion **54**, 124016 (2012).
2. A. A. Solodov, B. Yaakobi, D. H. Edgell, R. K. Follett, J. F. Myatt, C. Sorce, and D. H. Froula, Phys. Plasmas **23**, 102707 (2016).
3. R. Follett, "The Multiple-Beam Two-Plasmon-Decay Instability," Ph.D. thesis, University of Rochester, 2015.
4. Storage Phosphor Screen BAS-IP, GE Healthcare Bio-Sciences, Pittsburgh, PA 15264-3065, http://www.gelifesciences.com/webapp/wcs/stores/servlet/productById/en/GELifeSciences-us/28956474 (19 October 2017).
5. U. D. Chalasani, GE Healthcare Scientific Support, private communication (24 August 2017).
6. H. Ohuchi and L. C. Ha, Proc. Radiochim. Acta **1**, 49 (2011).
7. B. Hidding *et al.*, Rev. Sci. Instrum. **78**, 083301 (2007).
8. H. Ohuchi and A. Yamadera, Nucl. Instrum. Methods Phys. Res. A **490**, 573 (2002).
9. A. Taniyama, D. Shindo, and T. Oikawa, J. Electron. Microsc. **45**, 232 (1996).
10. T. Bonnet *et al.*, Rev. Sci. Instrum. **84**, 013508 (2013).
11. M. Thoms, Appl. Opt. **35**, 3702 (1996).
12. M. Thoms, Nucl. Instrum. Methods Phys. Res. A **378**, 598 (1996).

13. M. Thoms and H. von Seggern, J. Appl. Phys. **81**, 5887 (1997).

14. S. Vedantham and A. Karellas, IEEE Trans. Med. Imaging **29**, 790 (2010).

15. B. Maheu, J. N. Letoulouzan, and G. Gouesbet, Appl. Opt. **23**, 3353 (1984).

16. S. Masalovich *et al*., Nucl. Instrum. Methods Phys. Res. A **539**, 236 (2005).

17. G. J. Williams *et al*., Rev. Sci. Instrum. **85**, 11E604 (2014).

18. R. Paulavičius and J. Žilinskas, in *Simplicial Global Optimization*, SpringerBriefs in Optimization, edited by P. M. Pardalos *et al*. (Springer, New York, 2014), Chap. 1, pp. 1–19.

19. G. Boutoux *et al*., Rev. Sci. Instrum. **87**, 043108 (2016).

20. J. Allison *et al*., Nucl. Instrum. Methods Phys. Res. A **835**, 186 (2016).